



1 **Measurement-based modeling of daytime and nighttime oxidation of atmospheric mercury**

2

3 **Maor Gabay¹, Mordechai Peleg², Erick Fredj³, Eran Tas^{1*}**

4

5 ¹The Department of Soil and Water Sciences, The Robert H. Smith Faculty of Agriculture, Food
6 and Environment, Hebrew University of Jerusalem, Rehovot, Israel

7 ²Institute of Earth Sciences, Edmud Safra Campus, Givat Ram, The Hebrew University of
8 Jerusalem, Jerusalem 91904, Israel

9 ³Department of Computer Science, Jerusalem College of Technology, Jerusalem 91160, Israel

10

11

12

13

14

15

16

17 *Correspondence to: Eran Tas, The Department of Soil and Water Sciences, The Robert H. Smith
18 Faculty of Agriculture, Food and Environment, Hebrew University of Jerusalem, Rehovot, Israel.

19 eran.tas@mail.huji.ac.il.

20



21 **Abstract.** Accurate characterization of gaseous elemental mercury (GEM) chemical oxidation
22 pathways and their kinetics is critically important for assessing the transfer of atmospheric mercury
23 to bioaquatic systems. Recent comprehensive field measurements have suggested that the nitrate
24 radical (NO_3) plays a role in efficient nighttime oxidation of GEM, and that the role of the hydroxyl
25 radical (OH) as a GEM oxidant has been underestimated. We used the CAABA/MECCA chemical
26 box model and additional kinetic calculations to analyze these measurement results, in order to
27 investigate the nighttime and daytime oxidation of GEM. We assumed a second-order reaction for
28 the NO_3 induced nighttime oxidation of GEM. Our analysis demonstrated that nighttime oxidation of
29 GEM has to be included in the model to account for the measured variations in nighttime reactive
30 gaseous mercury (RGM) concentration. A lower limit and best-fit rate constant for GEM nighttime
31 oxidation are provided. To the best of our knowledge, this is the first time that a rate for nighttime
32 oxidation of GEM has been determined based on field measurements. Our analysis further indicates
33 that OH has a much more important role in GEM oxidation than commonly considered. A lower-
34 limit rate constant for the OH–RGM reaction is provided.

35

36 **1 Introduction**

37

38 Over 90% of atmospheric mercury is in the form of gaseous elemental mercury (GEM) (Schroeder
39 and Munthe, 1998). With a lifetime of 6 to 24 months, it is considered a global pollutant (Cole et al.,
40 2013). GEM oxidation to Hg^{2+} is associated with the formation of more reactive and soluble species,
41 either in the gaseous phase (reactive gaseous mercury, or RGM) or as particulate matter (fine



42 particulate-bound mercury, or FPM). RGM and FPM are deposited from the atmosphere much more
43 rapidly than GEM, by both dry and wet deposition.

44 Oxidation of GEM is therefore a critical stage in the process of transferring atmospheric
45 mercury to aquatic systems, where it can be further converted into the highly toxic biocumulative
46 methyl mercury (MeHg) (Schroeder and Munthe, 1998). Accurate characterization of GEM chemical
47 oxidation pathways and their kinetics is therefore highly important in assessing the transfer of
48 atmospheric mercury to bioaquatic systems. Even though many computer-modeling studies in recent
49 years have focused on investigating the oxidation and deposition of GEM, our understanding of the
50 related mechanisms is still far from complete (Subir et al., 2011). Uncertainty in mercury modeling
51 arises from several sources (Ariya et al., 2009, 2015), including incomplete information on chemical
52 reaction pathways and their kinetics (e.g., oxidation of GEM by NO_3 ; Peleg et al., 2015), poor
53 characterization of removal and recycling via heterogeneous processes (e.g., reduction of Hg(II) by
54 aqueous hydroperoxyl radical (HO_2); Lin and Pongprueksa, 2007), and removal via dry deposition
55 (Bergan and Rodhe, 2001; Lin and Pongprueksa, 2007). Uncertainties are also associated with
56 inaccurate mercury speciation (e.g., mercury oxide (HgO) speciation between the gas and particulate
57 phases; Hedgecock et al., 2005; Jaffe et al., 2014; Lu and Schroeder, 2004).

58 A major source of uncertainty in simulating the GEM oxidation pathway is inaccuracy in
59 oxidation-rate determinations. For instance, a sensitivity study by Bergan and Rodhe (2001) indicated
60 that the rate constant suggested by Hall (1995) for GEM oxidation by ozone (O_3) is too slow to
61 account for the major portion of GEM removal from the atmosphere. A different kinetics study, using
62 the Pal and Ariya (2004b) O_3 -GEM rate constant showed that the oxidation rate of GEM is too fast,



63 leading to unrealistically low GEM concentrations (Seigneur et al., 2006). Calvert and Lindberg
64 (2005) pointed out that direct oxidation of GEM by O_3 is unlikely in the atmosphere, and HgO
65 formation may occur via initial formation of HgO_3 . Whereas a laboratory study by Sommar et al.
66 (2001) suggested that the lifetime of GEM against oxidation by OH ranges from 4 to 7 months, other
67 studies have suggested that GEM removal by OH is probably unimportant in the atmosphere (Calvert
68 and Lindberg, 2005; Goodsite et al., 2004). These cardinal results reinforce the current uncertainty
69 with respect to GEM oxidation kinetics, and the need for further study. Disagreements in evaluated
70 oxidation rates are common across kinetics studies performed by different methods – experimental,
71 theoretical calculations, or computerized global or detailed chemical models (e.g., the rate constant
72 of GEM oxidation by OH; Bergan and Rodhe, 2001). Different experimental conditions may also
73 cause differences in oxidation rates from one study to the next (e.g., Hall, 1995; Pal and Ariya,
74 2004b). Furthermore, in many cases, experimentally based determinations of oxidation rate are
75 performed at much higher reactant concentrations and lower pressures than found in the atmosphere,
76 leading to increased uncertainty when extrapolated to typical atmospheric conditions (Subir et al.,
77 2011).

78 In the present study, we applied a chemical box model to study the nighttime and daytime
79 pathways and oxidation rates of GEM based on recent field measurements performed by Peleg et al.
80 (2015). Those field measurements included simultaneous NO_3 and speciated mercury quantification,
81 which allowed reinforcing the assumption that NO_3 can significantly oxidize GEM as originally
82 suggested by Platt and Heintz (1994) and Sommar et al. (1997). Peleg et al. (2015) further suggested
83 underestimation, in previous studies, of daytime GEM oxidation by OH as compared to GEM
84 oxidation by O_3 .



85

86 **2 Methods**

87

88 **2.1 Field measurements**

89

90 The model simulations were based on measurements performed in Jerusalem, Israel (31°47'N
91 35°13'E, 760 m above sea level) from 24 Jun to 2 Aug 2012. The measurements and their results are
92 briefly discussed below; more detailed information can be found in Peleg et al. (2015). The
93 measurement area can be characterized as an urban area under semiarid conditions, and the major
94 source of air pollution is transportation emissions. Possible Hg pollution sources are two major power
95 plants located some 80 km to the NW and 65 km to the SW. Note that no correlations were observed
96 across the entire measurement periods between RGM concentration and other atmospheric chemical
97 species (e.g., CO: $R^2 < 0.01$; SO₄: $R^2 < 0.01$; SO₂: $R^2 < 0.1$), or between RGM and meteorological
98 parameters ($R^2 < 0.01$ both for wind speed and wind direction). It is therefore unlikely that measured
99 RGM concentrations were significantly influenced directly by anthropogenic emissions, as is further
100 discussed by Peleg et al. (2015). As shown previously, high NO₃ levels are formed in Jerusalem,
101 driven by relatively strong photochemical activity (e.g., typical daylight O₃ levels are ~60 ppb; Peleg
102 et al., 2015) and dry conditions (average 42% during the day and 65% at night; Asaf et al., 2009).
103 Typical mercury levels in the area are 0.2 ppt, in agreement with typical rural and remote sites in the
104 northern hemisphere (Valente et al., 2007). All instrumentation was situated on a building rooftop at
105 the Hebrew University campus at Givat Ram. Measurements included quantification of GEM using



106 a Tekran model 2537B instrument (Tekran Inc., Toronto, Canada), and the same instrument was used
107 in conjunction with Tekran 1130 and 1135 instruments to quantify RGM and FPM, respectively. The
108 reported 5min limit of detection (LOD) for the 2537B is $<0.02 \text{ ng m}^{-3}$, with some potential
109 reservations for RGM and FPM (Peleg et al., 2015). A long-path differential optical absorption
110 spectrometer (LP-DOAS; Platt, 1994; Platt and Heintz, 1994; Sigrist, 1994) was used to quantify NO_3
111 with an average LOD of $8.7 \pm 5.2 \text{ ng m}^{-3}$.

112 Trace gases, including carbon monoxide, sulfur dioxide, and ozone, were measured using
113 models 48i, 43i, and 49C, respectively (all from Thermo Environmental Instruments Inc., Waltham,
114 MA, USA), with manufacturer-reported LODs of 4.0 ppm, 2.0 ppb and 1.0 ppb, respectively. A
115 meteorological station (Met One Instruments, was situated on the same rooftop to measure basic
116 meteorological parameters (wind speed, wind direction, temperature, pressure, relative humidity
117 (RH)) with LODs of 0.5 m s^{-1} , 5° , 0.4 K, 0.2 torr and 3%, respectively. Solar radiation data were
118 available for Jerusalem from the Israel Meteorological Service.

119

120 **2.1.1 Field measurement-based kinetic calculations**

121 The field measurement results were used to estimate the rate constants of GEM with OH
122 ($k[\text{OH}+\text{Hg}^0]$) and NO_3 ($k[\text{NO}_3+\text{Hg}^0]$), based on 27 selected measurement days, as explained in more
123 detail in Sect. S1 of the Supplement. Note that these calculated rate constants may be specifically
124 valid for the specific research area. The calculations, as well as additional analyses (see Sect. 3.2 and
125 3.3), make use of OH concentrations. Because OH concentrations were not available for the
126 measurement site, a theoretical diurnal OH profile was constructed for the respective days, based on



127 the assumed correlation between OH concentration and UV intensity (Smith et al., 2006; von Glasow
128 et al., 2002) and assuming that maximal OH concentration was 0.5 ppt, which is among the highest
129 concentrations reported for semi-polluted areas (see Sect. S1 of the Supplement; Stone et al., 2012).
130 The diurnal OH concentration was then calculated accordingly for 7 Jul 2012 based on the measured
131 UV intensity. The UV data were taken from a nearby weather station (Nayot, Jerusalem). Figure 1
132 presents the constructed diurnal profile of OH, as well as the average measured diurnal profiles of O₃
133 and RGM.

134

135 **2.2 Model simulations**

136

137 The CAABA/MECCA chemical box model (Sander et al., 2005, 2011) was used for the research
138 analyses. CAABA/MECCA uses explicit chemical mechanisms of gas- and aqueous-phase reactions,
139 as well as photochemical reactions and heterogeneous reactions for aerosols and clouds. Gas-aerosol
140 partitioning is based on Henry's law, subjected to kinetic limitations (Sander and Crutzen, 1996).
141 Formation and scavenging of aerosols are both included in the MECCA module. The chemical
142 mechanism accounts for species containing O, H, C, N, S, Cl, Br, I and Hg, with a total of 664
143 equations (186 gas phase, 266 aqueous phase, 154 heterogeneous, 58 photolysis). The default
144 chemical mechanism of MECCA is available at <http://www.mecca.messy-interface.org/>. MECCA
145 was used to study the oxidation of GEM in the troposphere by Obrist et al. (2011), Tas et al. (2012),
146 and Xie et al. (2008). The oxidation pathways of mercury are shown in Tables S1–4 (see Sect. S2 of



147 the Supplement). The reaction of GEM with NO_3 was added to the chemical mechanism, taking into
148 account the study by Sommar et al. (1997), and based on preliminary simulations (not shown).

149 The possibility of direct oxidation of GEM by NO_3 , however, is in contrast to recent
150 computational results presented by Dibble et al. (2012), which indicated that the bond energy of Hg-
151 ONO_2 is far too low to support direct oxidation by NO_3 . However, recent findings by Peleg et al.
152 (2015) suggest that NO_3 is directly involved in GEM oxidation. Therefore, while NO_3 may not act as
153 initiator of the GEM oxidation, it may play a role in a secondary addition to the first step of Hg
154 oxidation (XHg^\cdot). Because the mechanism by which NO_3 leads to GEM oxidation is currently
155 unknown, and taking into account the relatively strong correlation between RGM and NO_3 observed
156 by Peleg et al. (2015), as a first approximation we incorporated the nighttime oxidation of GEM by
157 NO_3 as a second-order rate according to the reaction:



159 We assumed that O_3 , OH, NO_3 , and H_2O_2 are the only GEM oxidants. While gas-phase bromine atom
160 (Br) may be the main viable GEM oxidant on a global scale, particularly over marine regions and the
161 free troposphere (Holmes et al., 2010), we assumed that its contribution to GEM oxidation at the
162 measurement site is relatively small. This assumption was based on previous measurements
163 performed at the Dead Sea basin, which indicated that no RGM is present when BrO levels decrease
164 to below the detection limit of the DOAS setup (~ 3 ppt; Obrist et al., 2011), combined with the fact
165 that no BrO was observed during DOAS measurements performed in Jerusalem (unpublished
166 results). Furthermore, Wang et al. (2016) indicated a lifetime of a few days for GEM with BrO
167 concentrations of a few parts per trillion, whereas the lifetime of GEM based on our study is much



168 shorter, reinforcing the notion that Br-induced oxidation of GEM does not play a significant role at
169 the measurement site.

170 The specific model simulations used for this study are summarized in Table 1. For the BASE
171 simulation, we used the model with one aerosol mode, representing sulfate aerosols. We configured
172 the model to account for a sulfate aerosol concentration of $8 \mu\text{g m}^{-3}$, based on a previous study in the
173 region (Andreae et al., 2002; Formenti et al., 2001; Wanger et al., 2000). Note, however, that the low
174 FPM concentrations observed at the measurement site suggest that only a relatively small portion of
175 the mercury species partitioned into the aerosol phase (Peleg et al., 2015). The relatively small effect
176 of aerosols in the studied area may result from the relatively low RH in the region. Simulations were
177 configured to represent typical meteorological conditions in the measurement area for temperature
178 (293 K), daytime boundary layer height (1000 m) and RH (42%). The GEM level was kept constant
179 at 210 ppq (the average measured concentration). A realistic representation of the photochemistry in
180 the model is highly important considering its direct impact on the daytime GEM oxidants OH and
181 O_3 , and the impact of O_3 concentrations on nighttime NO_3 concentrations (Asaf et al., 2010).
182 Therefore, special attention was given to ensure realistic representation of photochemistry in the
183 model by verifying that NO_3 , NO, NO_2 and O_3 concentrations agree with the corresponding measured
184 concentrations and volatile organic compounds (VOC) concentrations agree with typical suburban
185 concentrations (Finlayson-Pitts and Pitts Jr, 1999; see Figs. S3–S5 of the Supplement). This was
186 achieved by using adequate fixed values for the fluxes of NO, NO_2 and VOCs as boundary conditions
187 for the model during the simulations. Note that the maximum daytime simulated BASE O_3 reached
188 about 83 ppb, in agreement with the average over the corresponding measured values.



189 BASE was used with the rate constant for the oxidation of GEM by O₃ ($k[\text{O}_3+\text{Hg}^0]$) suggested
190 by Hall (1995). The PAL-ARIYA simulation used the $k[\text{O}_3+\text{Hg}^0]$ suggested by Pal and Ariya
191 (2004b). A set of simulations, HI-PHOT-CHM, used a daily maximal O₃ concentration of ~120 ppb,
192 instead of ~83 ppb. The set of simulations FIT used different combinations of rate constants for GEM
193 oxidation, based on the literature and measured RGM (Sect. S3 of the Supplement). The set of
194 simulations DRYDEP used dry deposition rates ranging from 0.1–5 cm s⁻¹ (Sect. S4 of the
195 Supplement).

196 Preliminary simulations indicated that while the GEM oxidation rates used in the model lead
197 to reasonable agreement of simulated HgO with the measured RGM for a single simulation day, the
198 day-to-day accumulation of RGM is overestimated by the model. We attribute this to underestimation
199 of nighttime HgO-removal processes, possibly due to lack of processes in the model accounting for
200 the uptake of RGM and/or FPM by wet surfaces other than aerosols. Instead of parameterizing these
201 removal processes into the model, we accounted for their effect on the daytime analyses by using a
202 $k[\text{NO}_3+\text{Hg}^0]$ value of 5.00E-17 cm³ molecule⁻¹ s⁻¹, which is lower than the value suggested by us
203 (2.0E-15–3.0E-15 cm³ molecule⁻¹ s⁻¹; see Sect. 3.3). Exceptional were the simulations PAL-ARIYA*
204 and BASE*, which were run with $k[\text{NO}_3+\text{Hg}^0]$ of 2.00E-15 and 3.00E-15, respectively (see Table 1),
205 and used to explore nighttime GEM oxidation.

206

207

208



209 **3 Results and discussion**

210

211 **3.1 Model evaluation**

212

213 In this section, we evaluate the model's ability to reproduce the observations, and test the sensitivity
214 of the model configuration to removal processes by aerosols, using the BASE and PAL-ARIYA
215 simulations. Analysis of the sensitivity to dry deposition is presented in Sect. S4 of the Supplement.

216

217 **3.1.1 GEM oxidation and reactive mercury partitioning**

218 In the marine boundary layer and the upper troposphere, GEM oxidation by reactive halogen species,
219 and in particular Br (Holmes et al., 2010; Lin et al., 2004), is considered a major sink for GEM on a
220 global scale. We do not expect to have substantial concentrations of halogens at the measurement site
221 due to its remoteness from the sea (see Sect. 2.2). Therefore, we did not include oxidation reactions
222 of GEM by reactive halogen species in the model. Previous studies have indicated that HgO can be
223 considered the main product of GEM reactions with OH, O₃, NO₃ and H₂O₂ (Pal and Ariya, 2004a,
224 2004b; Sommar et al., 2001). However, several studies have suggested that some of the produced
225 HgO might be considered Hg(s) due to its low vapor pressure and its fast uptake by aerosols
226 (Hedgecock et al., 2005; Lu and Schroeder, 2004; Schroeder and Munthe, 1998), or due to rapid
227 heterogeneous-induced oxidation mechanisms (e.g., see Stephens et al., 2012), which we address in
228 Sect. 3.1.2. Note that while our model includes GEM oxidation by H₂O₂, its role is not discussed in



229 the paper, considering its low average and maximum contribution to GEM oxidation: 0.64% and
230 6.58%, and 2.43% and 4.62%, during the day and at night, respectively.

231 Figure 1 shows high nighttime variability in the average measured diurnal profile of RGM,
232 with no clear pattern, reflecting the fact that nighttime oxidants NO_3 and O_3 do not show any clear
233 temporal pattern (Peleg et al., 2015). During the day, however, three distinct time periods, associated
234 with three local maxima in RGM concentrations, can be observed (see Fig. 1). The local maximum
235 in RGM level in the morning (~ 0700 h) could be due to vaporization of deposited mercury from wet
236 surfaces and/or from aerosols (green color in Fig. 1). The rapid increase in RGM between ~ 0800 and
237 1100 h is probably due to the corresponding increase in OH and/or O_3 . However, the subsequent
238 decrease in RGM between ~ 1200 and 1400 h followed by a later increase in RGM between ~ 1400
239 and 1600 h suggests that the higher peak at ~ 1100 h occurs predominantly due to oxidation of OH
240 (yellow color in Fig. 1), while the smaller peak at ~ 1600 h is predominantly due to oxidation by O_3
241 (red color in Fig. 1).

242 Figure 2 presents the diurnal concentrations of both RGM and the major GEM oxidants O_3 ,
243 OH, and NO_3 , for the BASE and PAL-ARIYA simulations, separated into daytime and nighttime
244 periods. The BASE and PAL-ARIYA simulations showed a daytime HgO peak, which can be related
245 mainly to oxidation of GEM by O_3 and OH. The nighttime HgO concentrations are dictated by the
246 prescribed $k[\text{NO}_3+\text{Hg}^0]$ used in the model to reproduce the average measured nighttime RGM
247 concentrations (see Sect. 3.3). Note that PAL-ARIYA and BASE were performed with a significantly
248 lower $k[\text{NO}_3+\text{Hg}^0]$ than the value evaluated in this study, to compensate for underestimation of
249 nighttime HgO-removal processes in our model, and avoid day-to-day accumulation of HgO (see



250 Sect. 2.2). These simulations are used to study only daytime GEM oxidation, and we used different
251 simulations to explore nighttime GEM oxidation (Sect. 3.3). The much lower HgO and FPM daytime
252 peaks obtained by the BASE and PAL-ARIYA simulations, compared to the measurements, suggests
253 that the daytime oxidation rates used by these simulations were significantly underestimated relative
254 to the actual rates. For PAL-ARIYA, O₃ was higher than BASE by a factor of ~3.6, leading to a RGM
255 peak at around ~1500 h, about 4 h later than the measured daytime RGM peak.

256 Figure 3 shows peak values of RGM and FPM to compare the measured and simulated RGM
257 and FPM daytime and nighttime partitioning for the BASE and PAL-ARIYA (daytime) and BASE*
258 and PAL-ARIYA* (nighttime) simulations. The measured daytime and nighttime RGM and FPM
259 peaks refer to the average, over their highest daytime and nighttime concentrations, for days on which
260 clear peaks in RGM concentrations were observed, with no association with changes in RH during
261 the day (27 days) or night (19 days).

262 According to Fig. 3, daytime partitioning between RGM and FPM was 62% and 38% for
263 BASE and 71% and 29% for PAL-ARIYA, as compared with the measurements: 86% and 14%,
264 respectively. The corresponding nighttime partitioning, using $k[\text{NO}_3 + \text{Hg}^0]$ of 2.00E-15 and 3.00E-
265 15 cm³ molecule⁻¹ s⁻¹ for PAL-ARIYA and BASE, respectively (see Sect. 3.3), was similar for PAL-
266 ARIYA (84% and 16%), BASE (87% and 13%) and the measurements (89% and 11%). Overall, Fig.
267 3 indicates relatively good agreement between simulated and measured gas-particle partitioning of
268 reactive mercury for both nighttime (<6%) and daytime (<25%). However, considering additional
269 removal processes for reactive mercury which are not taken into account by the model (Sect. 3.1.2)
270 and the potential underestimation of the measured FPM (e.g Feddersen et al., 2012), Fig. 3 may only



271 provide a rough understanding of the gas-particle partitioning of reactive mercury. Hence, the
272 combined effect of GEM oxidation rates and RGM removal by aerosols is studied in Sect. 3.2 and
273 3.3, on the basis of magnitude and time of appearance of the measured RGM peak.

274 Figure 3 shows that prescribing the nighttime RGM using $k[\text{NO}_3+\text{Hg}^0] = 2.00\text{E-}15 \text{ cm}^3$
275 $\text{molecule}^{-1} \text{ s}^{-1}$ for PAL-ARIYA and $k[\text{NO}_3+\text{Hg}^0] = 3.00\text{E-}15 \text{ cm}^3 \text{ molecule}^{-1} \text{ s}^{-1}$ for BASE led to
276 relatively good agreement with the measured RGM of 114% and 112%, respectively. The simulated
277 daytime RGM level remained low for PAL-ARIYA (42%) and BASE (12%) relative to the average
278 measured value. This suggests that the daytime oxidation in the model was underestimated, as will
279 be further discussed in Sect. 3.1.2 and 3.2, together with heterogeneous cycling and removal
280 processes.

281

282 3.1.2 Aqueous-phase processes

283 Aqueous-phase chemistry plays a significant role in the removal and recycling of atmospheric
284 mercury species (Amos et al., 2012; Ariya et al., 2015). HgO is highly soluble in water (Henry's Law
285 constant of $2.7 \times 10^{12} \text{ M atm}^{-1}$), and thus readily dissolves in aqueous aerosols and clouds (Selin et
286 al., 2007). While Fig. 3 demonstrates that inclusion of gas-aerosol exchange in the model can
287 reasonably explain the measured partitioning into RGM and FPM, there are other processes that may
288 have occurred during the measurements that are not well represented by the model, such as RGM
289 uptake by wet surfaces and nucleation. Removal by wet surfaces is expected to be more efficient
290 during the night when RH increases, and may explain the apparent underestimation of RGM removal
291 in the model (see Sect. 2.2). These removal processes are not taken into account by the model and



292 therefore, RGM removal may be underestimated, which may result in underestimation of the modeled
293 GEM oxidation rate, as discussed in Sect. 3.2 and 3.3. Considering the dry conditions at the
294 measurement site, and the relatively reasonable agreement of the partitioned reactive mercury into
295 gas and particulate phases (Fig. 3), we do not expect the absence of such processes in our model to
296 lead to a significant underestimation of GEM oxidation rate. In this study, we explore the role of
297 aerosols in RGM removal and recycling on the basis of RGM formation rate and timing of
298 appearance. First, we explore the overall potential impact of aerosols on oxidation product
299 concentration.

300 Simulation NOARSL was used to investigate the influence of aerosols on GEM oxidation
301 (see Table 1). NOARSL is similar to the BASE simulation, but lacks aerosol chemistry. The
302 NOARSL RGM concentrations were higher by about 50 ppq than the measured RGM, which required
303 an increase in the dry deposition rate of RGM to 5 cm s^{-1} , as compared with 0.5 cm s^{-1} (Mason and
304 Sheu, 2002) in the BASE scenario, to obtain the measured RGM concentrations. This suggests that
305 when aerosol activity is not included in the model, either the simulated removal processes in the gas
306 phase are too slow or the GEM oxidation rates are too high, or both, to account for RGM removal.

307 Overall, Sect. 3.1 demonstrates potentially high sensitivity of the evaluated GEM oxidation
308 rate to heterogeneous processes, including aerosol loading during the day, and apparently, additional
309 removal processes at night. Therefore, in the following we compare the simulated HgO with the
310 measured RGM under various combinations of aerosol loadings and GEM oxidation rates. The
311 evaluation of the rate constants is based on both magnitude and timing of appearance of HgO.



312 Ultimately, the evaluated simulated GEM oxidation rate is compared with the rate constants that were
313 calculated directly from the measurements.

314

315 **3.2 Daytime oxidation**

316

317 To investigate the efficiency of O_3 and OH in GEM oxidation, we used different combinations of
318 their rate constant with GEM, as well as different realistic photochemical activities and liquid water
319 contents (LWCs). Note that the different LWC values represent different integrated available volumes
320 for gas–aerosol partitioning and aerosol aqueous-phase reactions, which were indicated as potentially
321 having a large effect on our results (see Sect. 3.1.2).

322 Figure 4 shows the impact of using different combinations of $k[OH+Hg^0]$ and $k[O_3+Hg^0]$
323 (panels a and b) and LWCs (panels c and d) on daytime HgO concentrations. The measured average
324 diurnal RGM profile and the simulated concentrations of O_3 and OH obtained by PAL-ARIYA and
325 BASE are also presented in panels a and b, respectively. Note that the dashed line inside the box in
326 the upper panels indicates the average measured daytime RGM maximum (5.88 ppq; see Fig. 3) and
327 the time period during which it occurred (~0900–1300 h; see Fig. 1). The vertical dimension of the
328 box in the upper panels marks the corresponding standard deviation of the mean of the daytime
329 measured RGM maxima (0.53 ppq). Figures 4a and 4b indicate poor agreement of simulated HgO
330 with measured RGM for both PAL-ARIYA and BASE in terms of concentrations. In two simulations
331 with higher photochemical activity (HI-PHOT-CHM; see in Table 1), employing significantly higher
332 O_3 and OH, the simulated HgO values are significantly lower than the measured RGM (Figs. 4a and



333 4b). In all of these simulations, the maximum simulated HgO occurs at around 1500 h, significantly
334 later than the peak of the measured RGM, and well timed with the afternoon RGM peak which we
335 attribute to oxidation by ozone. Figures 4a and 4b show that the simulated OH peak is much closer
336 in time to the measured noontime RGM peak than both the simulated and measured ozone peaks.
337 This implies that $k[\text{OH} + \text{Hg}^0]$ is underestimated in our model relative to $k[\text{O}_3 + \text{Hg}^0]$. Indeed,
338 increasing $k[\text{OH} + \text{Hg}^0]$ to $6.5 \text{ E-}13$ and $9.0 \text{ E-}13 \text{ cm}^3 \text{ molecule}^{-1} \text{ s}^{-1}$ for PAL-ARIYA and BASE,
339 respectively, resulted in better agreement between measured and simulated RGM in terms of both
340 magnitude and timing of maximum occurrence (Figs. 4a and 4b).

341 Figures 4c and 4d investigate the impact of aerosol LWC on simulated HgO concentrations.
342 It is shown that a higher LWC is associated with lower HgO concentrations and earlier peaks. These
343 two effects are caused by more efficient uptake of HgO by aerosols when applying a higher LWC.
344 Applying a LWC value of $5 \mu\text{g m}^{-3}$ combined with $k[\text{OH} + \text{Hg}^0]$ of $1.5\text{E-}12 \text{ cm}^3 \text{ molecule}^{-1} \text{ s}^{-1}$ (Fig.
345 4a) and $1.8\text{E-}12 \text{ cm}^3 \text{ molecule}^{-1} \text{ s}^{-1}$ (Fig. 4b) for PAL-ARIYA and BASE scenarios, respectively, the
346 simulated HgO shows relatively good agreement with the simulated RGM in terms of both magnitude
347 (5.88 ppb) and timing of peak occurrence ($\sim 0900\text{--}1300 \text{ h}$). This suggests that if a higher aerosol LWC
348 occurs at the measurement site than the default value used in the present study ($1.08 \mu\text{g m}^{-3}$), the
349 $k[\text{OH} + \text{Hg}^0]$ may be much higher than the values suggested above of $9\text{E-}13$ and $6.5\text{E-}13 \text{ cm}^3$
350 $\text{molecule}^{-1} \text{ s}^{-1}$ for $k[\text{OH} + \text{Hg}^0]$. LWC lower than $1.08 \mu\text{g m}^{-3}$ is associated with late appearance of
351 the simulated HgO daytime peak (see Figs. 4c and 4d), making it unrealistic. Hence, we conclude
352 that based on our analyses, a value of $6.5\text{E-}13 \text{ cm}^3 \text{ molecule}^{-1} \text{ s}^{-1}$ can be considered a lower-limit rate
353 constant for $k[\text{OH} + \text{Hg}^0]$, even if the default LWC of $1.08 \mu\text{g m}^{-3}$ is incorrect. We suggest that this



354 value can be considered a lower limit because the derived daytime HgO peak only marginally fits
355 with the average daytime peak in terms of timing (Fig. 4a). In addition, we expect that the used OH
356 concentrations are either equal to or higher than the actual OH at the measurement site (see Sect. 2.1).
357 Note that this suggested lower-limit rate constant ($k[\text{OH}+\text{Hg}^0] = 6.5\text{E-}13 \text{ cm}^3 \text{ molecule}^{-1} \text{ s}^{-1}$) is larger
358 by a factor of ~ 7 than the conventional value suggested by Sommar et al. (2001).

359 The $k[\text{OH}+\text{Hg}^0]$ value calculated based on the measurement results (see Sect. S1 of the
360 Supplement) was found to be $2.8(\pm 0.5)\text{E-}13$ and $1.1(\pm 0.5)\text{E-}13 \text{ cm}^3 \text{ molecule}^{-1} \text{ s}^{-1}$, using the Hall
361 (1995) and Pal and Ariya (2004b) $k[\text{O}_3+\text{Hg}^0]$ values, respectively, with errors representing the
362 standard deviations of the mean. These rate constants are higher by a factor of only 1.2 and 3.2,
363 respectively, than the commonly used $k[\text{OH}+\text{Hg}^0]$. Note, however, that these calculated $k[\text{OH}+\text{Hg}^0]$
364 values do not take into account RGM-removal processes, which would cause the total formed RGM
365 to be much higher than the concentrations used for the kinetic calculations. This can result in
366 significant underestimation of $k[\text{OH}+\text{Hg}^0]$ by the kinetic calculations.

367 Figure 5 presents an additional set of simulations like those shown in Fig. 4, but with constant
368 $k[\text{OH}+\text{Hg}]$, and different aerosol LWCs, O_3 concentrations and $k[\text{O}_3+\text{Hg}^0]$ values according to PAL–
369 ARIYA and BASE simulations. The daytime HgO concentrations are presented for PAL–ARIYA and
370 BASE using different aerosol LWCs (Fig. 5a) and the same $k[\text{OH}+\text{Hg}^0]$ ($9.52\text{E-}14 \text{ cm}^3 \text{ molecule}^{-1}$
371 s^{-1} ; Sommar et al., 2001) combined with average and higher O_3 concentrations (see HI-PHOT-CHM
372 in Table 1) and varying values for $k[\text{O}_3+\text{Hg}^0]$ (Fig. 5b). Note that the dashed line inside the box in
373 the two panels of Fig. 5 indicate the average of the measured daytime RGM maximum levels (5.88
374 ppq; see Fig. 3) and the time during which they occurred ($\sim 0900 \text{ h}$ – 1300 h ; see Fig. 1). The vertical



375 dimension of the box in the upper panels marks the corresponding standard deviation of the mean of
376 the measured daytime RGM maxima (0.53 ppq).

377 Using $k[\text{O}_3+\text{Hg}^0]$ according to Hall (1995) yields HgO concentrations similar to those
378 obtained when $k[\text{O}_3+\text{Hg}^0] = 0$. PAL-ARIYA provides significantly higher HgO, but it is still much
379 lower than the compatible RGM concentrations (Fig. 5b). The simulated daytime HgO peak is similar
380 to the compatible measured RGM concentrations only for simulations using the highest $k[\text{O}_3+\text{Hg}^0]$
381 value of $1.8\text{E-}18 \text{ cm}^3 \text{ molecule}^{-1} \text{ s}^{-1}$, about 1.5 orders of magnitude larger than Pal and Ariya's
382 (2004b) rate constant. Moreover, the timing of the daytime peak, in this case, occurs later than
383 actually observed. We checked whether a combination of higher $k[\text{O}_3+\text{Hg}^0]$ ($5\text{E-}18 \text{ cm}^3 \text{ molecule}^{-1}$
384 s^{-1}) and relatively high LWC ($5 \mu\text{g m}^{-3}$) would result in a more realistic HgO profile. The resulting
385 maximum HgO concentrations were similar to the compatible measured RGM maximum
386 concentration, but still peaked several hours later than the measured HgO (Fig. 5a).

387 Overall, lowering LWC resulted in a large delay in the simulated HgO peak compared with
388 the compatible measured RGM, while increasing LWC resulted in an HgO value that is too low.
389 Figure 5 therefore indicates that the observed RGM concentrations cannot be reproduced by the
390 model when using a combination of different higher $k[\text{O}_3+\text{Hg}^0]$ values and LWCs, and that the
391 underestimation of the daytime HgO formation is predominantly due to using too low a value for
392 $k[\text{OH}+\text{Hg}^0]$, rather than to inaccuracies in $k[\text{O}_3+\text{Hg}^0]$. Overall, Figs. 4 and 5 suggest that reasonable
393 reproduction of the measured RGM can only be achieved by significantly reducing the commonly
394 used $k[\text{O}_3+\text{Hg}^0]$ with respect to $k[\text{OH}+\text{Hg}^0]$ (see also Sect. S3 of the Supplement).

395



396 3.3 Nighttime oxidation

397

398 There is no published information available regarding the oxidation rate of GEM by NO₃ except for
399 the upper limit of 4E-15 cm³ molecule⁻¹ s⁻¹ suggested by Sommar et al. (1997). To investigate GEM
400 oxidation by NO₃, simulations were performed using a k[OH+Hg⁰] of 9.52E-14 cm³ molecule⁻¹ s⁻¹
401 as proposed by Sommar et al. (2001), both k[O₃+Hg⁰] values from Hall (1995) and Pal and Ariya
402 (2004b), and varying LWC values. The simulation day used the BASE* conditions, representing a
403 day with average O₃ concentrations (peaking at ~83 ppb) and a nighttime peak NO₃ of ~78 ppt. The
404 NO₃ peak value represents the average over measured NO₃ peaks at night, with relatively high peak
405 NO₃ concentrations (>60 ppt) that were associated with simultaneous RGM peaks. The average
406 concentrations of these RGM peaks equals 6.17 ppq, as indicated by the dashed horizontal lines in
407 Fig. 6. The vertical dimension of the shaded rectangle marks the corresponding standard deviation of
408 the mean of these RGM peaks (0.95 ppq).

409 Best agreement with the measured RGM concentrations was obtained when a value of 2.00E-
410 15 cm³ molecule⁻¹ s⁻¹ and 3.00E-15 cm³ molecule⁻¹ s⁻¹ was used with the k[O₃+Hg⁰] values from Pal
411 and Ariya (2004b) and Hall (1995), respectively. This suggests that k[NO₃+Hg⁰] = 2E-15 cm³
412 molecule⁻¹ s⁻¹ can be considered the lower limit for the oxidation rate of Hg⁰ involving NO₃. The
413 calculated k[NO₃+Hg⁰] was 2.8 (±0.5) E-15 cm³ molecule⁻¹ s⁻¹ using Hall's k[O₃+Hg⁰], and 1.9 (±0.5)
414 E-15 cm³ molecule⁻¹ s⁻¹ using Pal and Ariya's k[O₃+Hg⁰], with errors representing the standard
415 deviations of the mean.



416 Figure 6 further indicates that nighttime HgO concentrations span an order of magnitude for
417 LWCs ranging from 0.5–5 $\mu\text{g m}^{-3}$, implying that changes in RH and aerosol concentration could
418 significantly impact this estimated lower rate limit for $k[\text{NO}_3+\text{Hg}^0]$. Nevertheless, considering that
419 our analyses indicate underestimation of RGM-removal processes during the night in our model, we
420 do not expect the nighttime LWC at the site to be lower than that used by the default PAL-ARIYA
421 simulation (i.e., 1.08 $\mu\text{g m}^{-3}$). Therefore, we suggest that because heterogeneous processes can
422 significantly impact RGM removal, $2\text{E-}15 \text{ cm}^3 \text{ molecule}^{-1} \text{ s}^{-1}$ may be considered the lower limit for
423 the oxidation rate of Hg^0 involving NO_3 .

424

425 **4 Summary and conclusions**

426

427 **4.1 Daytime oxidation**

428

429 The oxidation rates proposed for GEM by ozone span 22 orders of magnitude, ranging from E-40 to
430 E-18 $\text{cm}^3 \text{ molecule}^{-1} \text{ s}^{-1}$ (Subir et al., 2011). In the present study, we chose two rate constants at the
431 high end of the scale: $3.11\text{E-}20 \text{ cm}^3 \text{ molecule}^{-1} \text{ s}^{-1}$ as proposed by Hall (1995), and $7.5\text{E-}19 \text{ cm}^3$
432 $\text{molecule}^{-1} \text{ s}^{-1}$ from Pal and Ariya (2004b), which are the most commonly used values in GEM
433 oxidation modeling (Subir et al., 2011). Our measurement-based modeling showed that neither of
434 these rate constants can reproduce the measured daytime and nighttime GEM oxidation rates. Best
435 agreement with measured results, in terms of both magnitude and timing, were obtained using a
436 $k[\text{OH}+\text{Hg}^0]$ of at least $6.5\text{-}9\text{E-}13 \text{ cm}^3 \text{ molecule}^{-1} \text{ s}^{-1}$. Based on our analyses, we suggest that this



437 value, which is higher by a factor of at least 7 than the rate constant suggested by Sommar et al.
438 (2001), should be considered the lower limit rate for the oxidation of Hg^0 by OH. Our analyses further
439 suggest that the actual rate for this process is probably higher, considering the timing of the
440 appearance of the simulated HgO peak compared with the measured RGM. The two $k[\text{O}_3+\text{Hg}^0]$
441 values tested, $3.11\text{E-}20 \text{ cm}^3 \text{ molecule}^{-1} \text{ s}^{-1}$ and $7.5\text{E-}19 \text{ cm}^3 \text{ molecule}^{-1} \text{ s}^{-1}$, seem to overestimate the
442 actual $k[\text{O}_3+\text{Hg}^0]$, in agreement with Calvert and Lindberg (2005). It is possible, however, that O_3
443 plays a significant role in GEM oxidation via heterogeneous processes, as suggested by previous
444 studies (e.g., Stephens et al., 2012), such that the overall oxidation rate of GEM by O_3 was
445 underestimated in our study. Nevertheless, our simulations demonstrate the unlikelihood of the strong
446 noontime RGM peak being explained by a higher GEM oxidation rate by O_3 . Based on our analyses,
447 the only explanation for this peak is a higher oxidation rate by OH than is commonly used.

448 The calculated $k[\text{OH}+\text{Hg}^0]$ based on the measurement results was found to be $2.8(\pm 0.5)\text{E-}13$
449 and $1.1(\pm 0.5)\text{E-}13 \text{ cm}^3 \text{ molecule}^{-1} \text{ s}^{-1}$ using the $k[\text{O}_3+\text{Hg}^0]$ values from Hall (1995) and Pal and
450 Ariya (2004b), respectively. These values, which agree with the theoretical $3.2 \text{ E-}13 \text{ cm}^3 \text{ molecule}^{-1}$
451 s^{-1} (Goodsite et al., 2004), represent lower limits, because they do not take into account any RGM-
452 removal processes (see Sect. 3.2). The calculated value agrees with the theoretical rate constant of
453 $3.2 \text{ E-}13 \text{ cm}^3 \text{ molecule}^{-1} \text{ s}^{-1}$ (Goodsite et al., 2004), rather than the rate constant of $9\text{--}12\text{E-}14 \text{ cm}^3$
454 $\text{ molecule}^{-1} \text{ s}^{-1}$ or lower, which was suggested based on previous experimental studies (Bauer et al.,
455 2003; Pal and Ariya, 2004a; Sommar et al., 2001) and is commonly used in models (Subir et al.,
456 2011).

457



458 4.2 Nighttime oxidation

459

460 To the best of our knowledge, no published information regarding the rate of GEM oxidation by NO₃
461 is currently available except for a suggested upper limit of 4E-15 cm³ molecule⁻¹ s⁻¹ (Sommar et al.,
462 1997).

463 Peleg et al. (2015) used measured data to show the correlation between NO₃ and RGM,
464 suggesting that NO₃ plays an important role in nighttime GEM oxidation. As far as we know, this is
465 the first paper to provide an estimation for nighttime NO₃-induced GEM oxidation based on field
466 measurements. Using these measurements, our modeling analyses indicated a lower-limit rate
467 constant of about 2.0E-15 cm³ molecule⁻¹ s⁻¹ NO₃, and 3.0E-15 cm³ molecule⁻¹ s⁻¹ for GEM oxidation
468 by NO₃ together with the k[O₃+Hg⁰] values of 3.11E-20 and 7.5E-19 cm³ molecule⁻¹ s⁻¹, respectively.
469 The calculated k[NO₃+Hg⁰] based directly on the measurement results was found to be 2.8(±0.5)E-
470 15 and 1.9(±0.5)E-15 cm³ molecule⁻¹ s⁻¹ using the k[O₃+Hg⁰] values from Hall (1995) and from Pal
471 and Ariya (2004b), respectively.

472 The present study indicates that nighttime oxidation of GEM by NO₃ must be taken into
473 account in GEM oxidation calculations, and that the importance of OH as a GEM oxidant is probably
474 higher than previously assumed. However, the impact of the relatively rapid oxidation of GEM by
475 NO₃ and OH indicated in the present study may vary in regions with different conditions, indicating
476 the need for future studies of GEM oxidation. In particular, the present study was performed under
477 relatively dry conditions. Under the influence of high RH levels (>50%), lower concentrations of NO₃
478 and OH are expected, together with higher recycling and scavenging of oxidized mercury products



479 due to the increase in aerosol activity. Therefore, this study emphasizes the need for future study of
480 GEM-oxidation pathways using detailed heterogeneous models.

481

482 **5. Data availability**

483 The data of this paper are available upon request. Please contact the corresponding author Eran Tas
484 (eran.tas@mail.huji.ac.il).

485

486 *Acknowledgements:* We wish to thank deeply Menachem Luria for motivating us to publish this
487 research. We thank Menachem Luria, Valeri Matveev, Daniel Obrist and Chris Moore for their
488 contribution to obtaining the measurement results which were used for the present study. E.T. holds
489 the Joseph H. and Belle R. Braun Senior Lectureship in Agriculture.

490

491 **References**

492

493 Amos, H. M., Jacob, D. J., Holmes, C., Fisher, J. A., Wang, Q., Yantosca, R. M., Corbitt, E. S.,
494 Galarneau, E., Rutter, A. and Gustin, M.: Gas-particle partitioning of atmospheric Hg (II) and its
495 effect on global mercury deposition, *Atmos. Chem. Phys.*, 12, 591-603, 2012.

496 Andreae, T. W., Andreae, M. O., Ichoku, C., Maenhaut, W., Cafmeyer, J., Karnieli, A. and
497 Orlovsky, L.: Light scattering by dust and anthropogenic aerosol at a remote site in the Negev
498 desert, Israel, *J. Geophys. Res.-Atmos.*, 107, AAC 3-1-AAC 3-18, 2002.



- 499 Ariya, P. A., Peterson, K., Snider, G. and Amyot, M.: Mercury chemical transformations in the gas,
500 aqueous and heterogeneous phases: state-of-the-art science and uncertainties, in: Mercury fate
501 and transport in the global atmosphere, Springer, 459-501, 2009.
- 502 Ariya, P. A., Amyot, M., Dastoor, A., Deeds, D., Feinberg, A., Kos, G., Poulain, A., Ryjkov, A.,
503 Semeniuk, K. and Subir, M.: Mercury Physicochemical and Biogeochemical Transformation in
504 the Atmosphere and at Atmospheric Interfaces: A Review and Future Directions, Chem. Rev.,
505 2015.
- 506 Asaf, D., Pedersen, D., Matveev, V., Peleg, M., Kern, C., Zingler, J., Platt, U. and Luria, M.: Long-
507 term measurements of NO₃ radical at a semiarid urban site: 1. extreme concentration events and
508 their oxidation capacity, Environ. Sci. Technol., 43, 9117-9123, 2009.
- 509 Asaf, D., Tas, E., Pedersen, D., Peleg, M. and Luria, M.: Long-term measurements of NO₃ radical
510 at a semiarid urban site: 2. Seasonal trends and loss mechanisms, Environ. Sci. Technol., 44,
511 5901-5907, 2010.
- 512 Bauer, D., D'Ottone, L., Campuzano-Jost, P. and Hynes, A.: Gas phase elemental mercury: a
513 comparison of LIF detection techniques and study of the kinetics of reaction with the hydroxyl
514 radical, J. Photochem. Photobiol. A., 157, 247-256, 2003.
- 515 Bergan, T. and Rodhe, H.: Oxidation of elemental mercury in the atmosphere; Constraints imposed
516 by global scale modelling, J. Atmos. Chem., 40, 191-212, 2001.
- 517 Calvert, J. G. and Lindberg, S. E.: Mechanisms of mercury removal by O₃ and OH in the
518 atmosphere, Atmos. Environ., 39, 3355-3367, 2005.



- 519 Cole, A., Steffen, A., Pfaffhuber, K., Berg, T., Pilote, M., Poissant, L., Tordon, R. and Hung, H.:
- 520 Ten-year trends of atmospheric mercury in the high Arctic compared to Canadian sub-Arctic and
- 521 mid-latitude sites, *Atmos. Chem. Phys.*, 13, 1535-1545, 2013.
- 522 Dibble, T., Zelic, M. and Mao, H.: Thermodynamics of reactions of ClHg and BrHg radicals with
- 523 atmospherically abundant free radicals, *Atmos. Chem. Phys.*, 12, 10271-10279, 2012.
- 524 Feddersen, D., Talbot, R., Mao, H. and Sive, B.: Size distribution of particulate mercury in marine
- 525 and coastal atmospheres, *Atmos. Chem. Phys.*, 12, 10899-10909, 2012.
- 526 Finlayson-Pitts, B. J. and Pitts Jr, J. N.: Chemistry of the upper and lower atmosphere: theory,
- 527 experiments, and applications, Academic press, 1999.
- 528 Formenti, P., Andreae, M., Andreae, T., Ichoku, C., Schebeske, G., Kettle, J., Maenhaut, W.,
- 529 Cafmeyer, J., Ptasinsky, J. and Karnieli, A.: Physical and chemical characteristics of aerosols
- 530 over the Negev Desert (Israel) during summer 1996, *J. Geophys. Res.-Atmos.*, 106, 4871-4890,
- 531 2001.
- 532 Goodsite, M. E., Plane, J. and Skov, H.: A theoretical study of the oxidation of Hg⁰ to HgBr₂ in the
- 533 troposphere, *Environ. Sci. Technol.*, 38, 1772-1776, 2004.
- 534 Hall, B.: The gas phase oxidation of elemental mercury by ozone, in: *Mercury as a Global*
- 535 *Pollutant*, Springer, 301-315, 1995.
- 536 Hedgecock, I. M., Trunfio, G. A., Pirrone, N. and Sprovieri, F.: Mercury chemistry in the MBL:
- 537 Mediterranean case and sensitivity studies using the AMCOTS (Atmospheric Mercury
- 538 Chemistry over the Sea) model, *Atmos. Environ.*, 39, 7217-7230, 2005.



- 539 Holmes, C. D., Jacob, D. J., Corbitt, E. S., Mao, J., Yang, X., Talbot, R. and Slemr, F.: Global
540 atmospheric model for mercury including oxidation by bromine atoms, *Atmos. Chem. Phys.*, 10,
541 12037-12057, 2010.
- 542 Jaffe, D. A., Lyman, S., Amos, H. M., Gustin, M. S., Huang, J., Selin, N. E., Levin, L., Ter Schure,
543 A., Mason, R. P. and Talbot, R.: Progress on understanding atmospheric mercury hampered by
544 uncertain measurements, *Environ. Sci. Technol.*, 48, 7204-7206, 2014.
- 545 Lin, C. and Pongprueksa, P.: Scientific uncertainties in atmospheric mercury models II: Sensitivity
546 analysis in the CONUS domain, *Atmos. Environ.*, 41, 6544-6560, 2007.
- 547 Lin, C., Pongprueksa, P., Ho, T. C., Chu, H. and Jang, C.: Development of mercury modeling
548 schemes within CMAQ framework: science and model implementation issues, *Molecules*, 900,
549 3, 2004.
- 550 Lu, J. Y. and Schroeder, W. H.: Annual time-series of total filterable atmospheric mercury
551 concentrations in the Arctic, *Tellus B*, 56, 213-222, 2004.
- 552 Mason, R. P. and Sheu, G.: Role of the ocean in the global mercury cycle, *Global Biogeochem.*
553 *Cycles*, 16, 40-1-40-14, 2002.
- 554 Obrist, D., Tas, E., Peleg, M., Matveev, V., Faïn, X., Asaf, D. and Luria, M.: Bromine-induced
555 oxidation of mercury in the mid-latitude atmosphere, *Nature Geoscience*, 4, 22-26, 2011.
- 556 Pal, B. and Ariya, P. A.: Gas-phase HO-initiated reactions of elemental mercury: kinetics, product
557 studies, and atmospheric implications, *Environ. Sci. Technol.*, 38, 5555-5566, 2004a.
- 558 Pal, B. and Ariya, P. A.: Studies of ozone initiated reactions of gaseous mercury: kinetics, product
559 studies, and atmospheric implications, *Physical Chemistry Chemical Physics*, 6, 572-579, 2004b.



- 560 Peleg M, Tas E, Obrist D, Matveev V, Moore C, Gabay M, Luria M.:
561 Observational Evidence for Involvement of Nitrate Radicals in Nighttime Oxidation of Mercury,
562 Environmental Science & Technology, 2015.
- 563 Platt, U.: Differential optical absorption spectroscopy (DOAS), Air Monitoring by Spectroscopic
564 Technique, 127, 27-84, 1994.
- 565 Platt, U. and Heintz, F.: Nitrate radicals in tropospheric chemistry, Isr. J. Chem., 34, 289-300, 1994.
- 566 Sander, R. and Crutzen, P. J.: Model study indicating halogen activation and ozone destruction in
567 polluted air masses transported to the sea, J. Geophys. Res.-Atmos., 101, 9121-9138, 1996.
- 568 Sander, R., Kerkweg, A., Jöckel, P. and Lelieveld, J.: Technical note: The new comprehensive
569 atmospheric chemistry module MECCA, Atmos. Chem. Phys., 5, 445-450, 2005.
- 570 Sander, R., Baumgaertner, A., Gromov, S., Harder, H., Jöckel, P., Kerkweg, A., Kubistin, D.,
571 Regelin, E., Riede, H. and Sandu, A.: The atmospheric chemistry box model CAABA/MECCA-
572 3.0, Geoscientific Model Development, 4, 373-380, 2011.
- 573 Schroeder, W. H. and Munthe, J.: Atmospheric mercury—an overview, Atmos. Environ., 32, 809-
574 822, 1998.
- 575 Seigneur, C., Vijayaraghavan, K. and Lohman, K.: Atmospheric mercury chemistry: Sensitivity of
576 global model simulations to chemical reactions, J. Geophys. Res.-Atmos., 111, PAGES, 2006.
- 577 Selin, N. E., Jacob, D. J., Park, R. J., Yantosca, R. M., Strode, S., Jaeglé, L. and Jaffe, D.: Chemical
578 cycling and deposition of atmospheric mercury: Global constraints from observations, J.
579 Geophys. Res.-Atmos., 112, PAGES, 2007.



- 580 Sigrist, M. W.: Differential optical absorption spectroscopy (DOAS), in Air monitoring by
581 spectroscopic techniques, John Wiley & Sons, 1994.
- 582 Smith, S., Lee, J., Bloss, W., Johnson, G., Ingham, T. and Heard, D.: Concentrations of OH and HO
583 2 radicals during NAMBLEX: measurements and steady state analysis, Atmos. Chem. Phys., 6,
584 1435-1453, 2006.
- 585 Sommar, J., Hallquist, M., Ljungström, E. and Lindqvist, O.: On the gas phase reactions between
586 volatile biogenic mercury species and the nitrate radical, J. Atmos. Chem., 27, 233-247, 1997.
- 587 Sommar, J., Gårdfeldt, K., Strömberg, D. and Feng, X.: A kinetic study of the gas-phase reaction
588 between the hydroxyl radical and atomic mercury, Atmos. Environ., 35, 3049-3054, 2001.
- 589 Stephens, C. R., Shepson, P. B., Steffen, A., Bottenheim, J. W., Liao, J., Huey, L. G., Apel, E.,
590 Weinheimer, A., Hall, S. R. and Cantrell, C.: The relative importance of chlorine and bromine
591 radicals in the oxidation of atmospheric mercury at Barrow, Alaska, J. Geophys. Res.-Atmos.,
592 117, PAGES, 2012.
- 593 Stone, D., Whalley, L. K. and Heard, D. E.: Tropospheric OH and HO₂ radicals: field
594 measurements and model comparisons, Chem. Soc. Rev., 41, 6348-6404, 2012.
- 595 Subir, M., Ariya, P. A. and Dastoor, A. P.: A review of uncertainties in atmospheric modeling of
596 mercury chemistry I. Uncertainties in existing kinetic parameters—Fundamental limitations and
597 the importance of heterogeneous chemistry, Atmos. Environ., 45, 5664-5676, 2011.
- 598 Tas, E., Obrist, D., Peleg, M., Matveev, V., Fain, X., Asaf, D. and Luria, M.: Measurement-based
599 modelling of bromine-induced oxidation of mercury above the Dead Sea, Atmos. Chem. Phys.,
600 12, 2429-2440, 2012.



601 Valente, R. J., Shea, C., Lynn Humes, K. and Tanner, R. L.: Atmospheric mercury in the Great
602 Smoky Mountains compared to regional and global levels, Atmos. Environ., 41, 1861-1873,
603 2007.

604 von Glasow, R., Sander, R., Bott, A. and Crutzen, P. J.: Modeling halogen chemistry in the marine
605 boundary layer 1. Cloud-free MBL, J. Geophys. Res.-Atmos., 107, ACH 9-1-ACH 9-16, 2002.

606 Wang, C., Wang, Z., Ci, Z., Zhang, X. and Tang, X.: Spatial-temporal distributions of gaseous
607 element mercury and particulate mercury in the Asian marine boundary layer, Atmos. Environ.,
608 126, 107-116, 2016.

609 Wanger, A., Peleg, M., Sharf, G., Mahrer, Y., Dayan, U., Kallos, G., Kotroni, V., Lagouvardos, K.,
610 Varinou, M. and Papadopoulos, A.: Some observational and modeling evidence of long-range
611 transport of air pollutants from Europe toward the Israeli coast, J. Geophys. Res.-Atmos., 105,
612 7177-7186, 2000.

613 Xie, Z., Sander, R., Pöschl, U. and Slemr, F.: Simulation of atmospheric mercury depletion events
614 (AMDEs) during polar springtime using the MECCA box model, Atmos. Chem. Phys., 8, 7165-
615 7180, 2008.

616

617

618

619

620

621



622 **Table 1.** Key to different simulation types.

Simulation/ s name	$K [O_3+Hg^0]$ [cm ³ molecule ⁻¹ s ⁻¹]	$K [OH+Hg^0]$ [cm ³ molecule ⁻¹ s ⁻¹]	$K [NO_3+Hg^0]$ [cm ³ molecule ⁻¹ s ⁻¹]	Sulfate aerosol LWC [μg m ⁻³]	Dry deposition [cm s ⁻¹]	O ₃ daily maximum [ppb]
BASE	3.11E-20 ^a	9.52E-14 ^b	5.00E-17	1.08	0.5 ^c	83
BASE*	3.11E-20	9.52E-14	3.00E-15	1.08	0.5	83
NOARSL	3.11E-20	9.52E-14	5.00E-17	Non	0.5	83
PAL- ARIYA	7.50E-19 ^d	9.52E-14	5.00E-17	1.08	0.5	83
PAL- ARIYA*	7.50E-19	9.52E-14	2.00E-15	1.08	0.5	83
Liquid water content (LWC)	3.11E-20 – 5E-18	9.52E-14 – 1.8E-12	5.00E-17 ,2.00E-15	LWC= 0.5-5	LWC	3.11E-20 – 5E-18
DRYDEP	3.11E-20	9.52E-14	-	1.08	0.1-5	83
HI-PHOT- CHM	3.11E-20, 7.5E-19	9.52E-14	5.00E-17 (day) ,2.00E-15 (night)	1.08	0.5	120
FIT	3.11E-20, 7.50E-19, 1.80E-18	9.52E-14, 9.00E-13, 6.50E-13	1.60E-15, 2.30E-15,1.50E-16	1.08	0.5	83

623 ^aHall (1995).

624 ^bSommar et al. (2001)

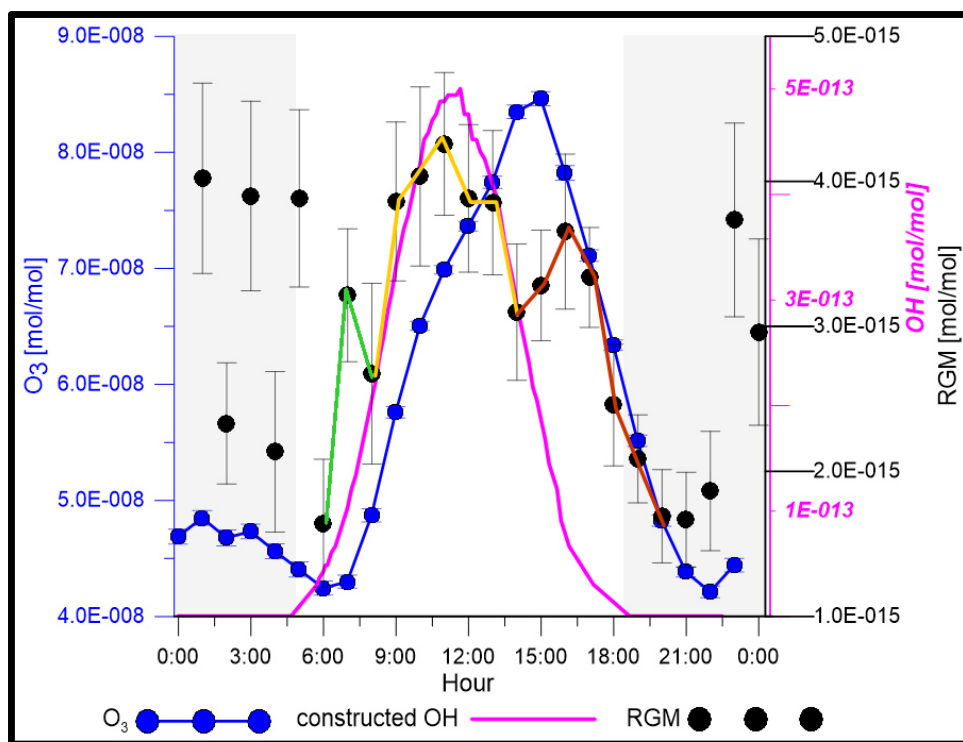
625 ^cMason and Sheu (2002).

626 ^dPal and Ariya (2004b).

627



628



629

630 **Figure 1.** Ozone and RGM hourly average measured concentrations and OH constructed concentration. The
631 vertical lines represent the standard deviation of the mean for the measured O₃ and RGM concentrations. The
632 shaded areas indicate nighttime. The highest average measured daytime RGM levels coincide with the
633 constructed OH peak, rather than with the O₃ peak. The average hourly daytime RGM concentrations are
634 marked by three different colors, indicating three distinct time periods, 0600–0800 h (green), 0800–1400 h
635 (yellow), 1400–2000 h (red), which were apparently controlled by different processes (see Sect. 3.1.1).

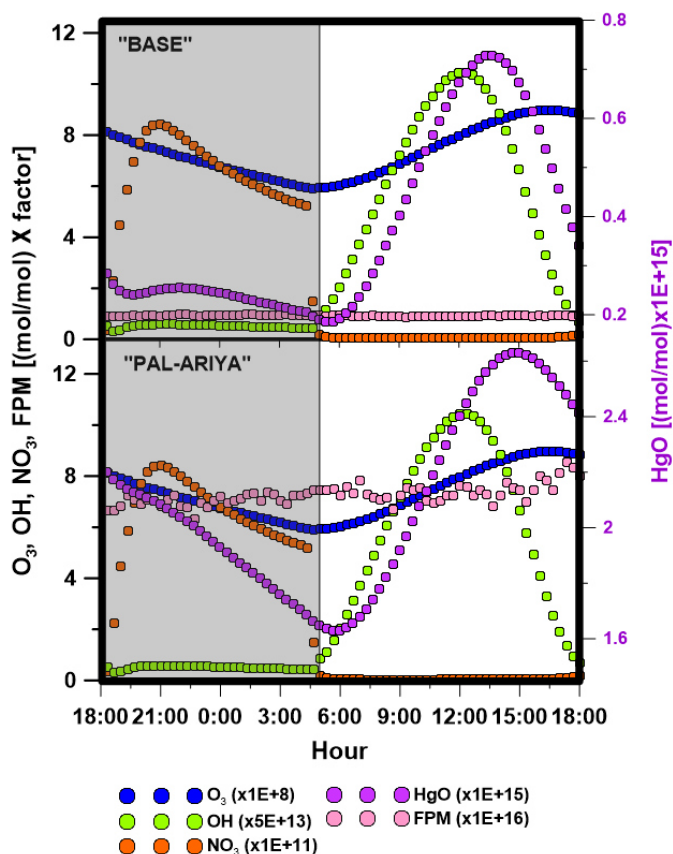
636

637

638



639

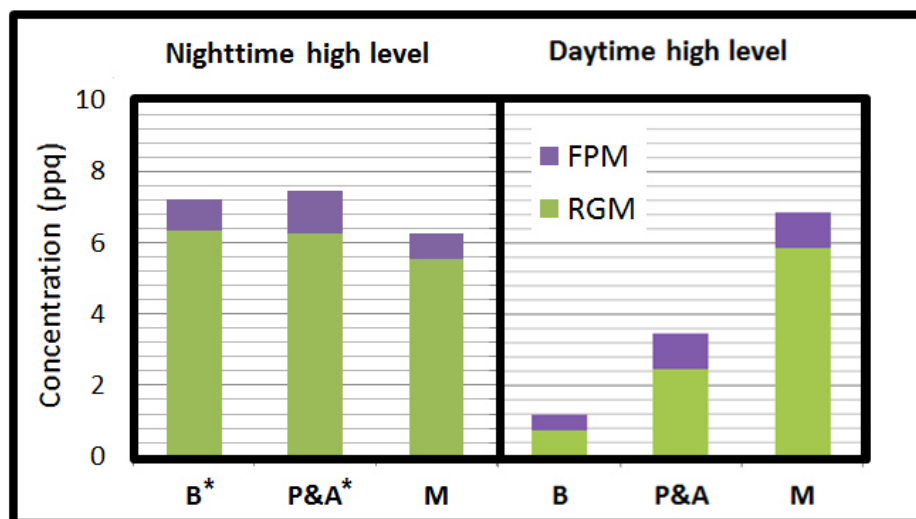


655 **Figure 2.** Simulated diurnal profile of major GEM oxidants and oxidation products used in the model.
656 Presented are the diurnal profiles of the GEM oxidants O_3 , OH and NO_3 used in the model, multiplied by a
657 factor of $1E+8$, $5E+13$ and $1E+11$, respectively, together with the diurnal profiles of the oxidation products
658 RGM and FPM, multiplied by a factor of $1E+15$ and $1E+16$, respectively. The concentrations are presented
659 for both the BASE simulation (upper panel) and PAL-ARIYA simulation (lower panel). GEM was kept
660 constant at 210 ppq (not shown here).

661



662



663

664 **Figure 3.** Concentration and partitioning of the oxidized Hg. Average measured (M) maximum daytime and
665 nighttime levels of FPM and RGM are presented versus the compatible simulated concentrations, which were
666 obtained by BASE (B)/BASE* (B*) and PAL-ARIYA (P&A)/PAL-ARIYA* (P&A*).

667

668

669

670

671

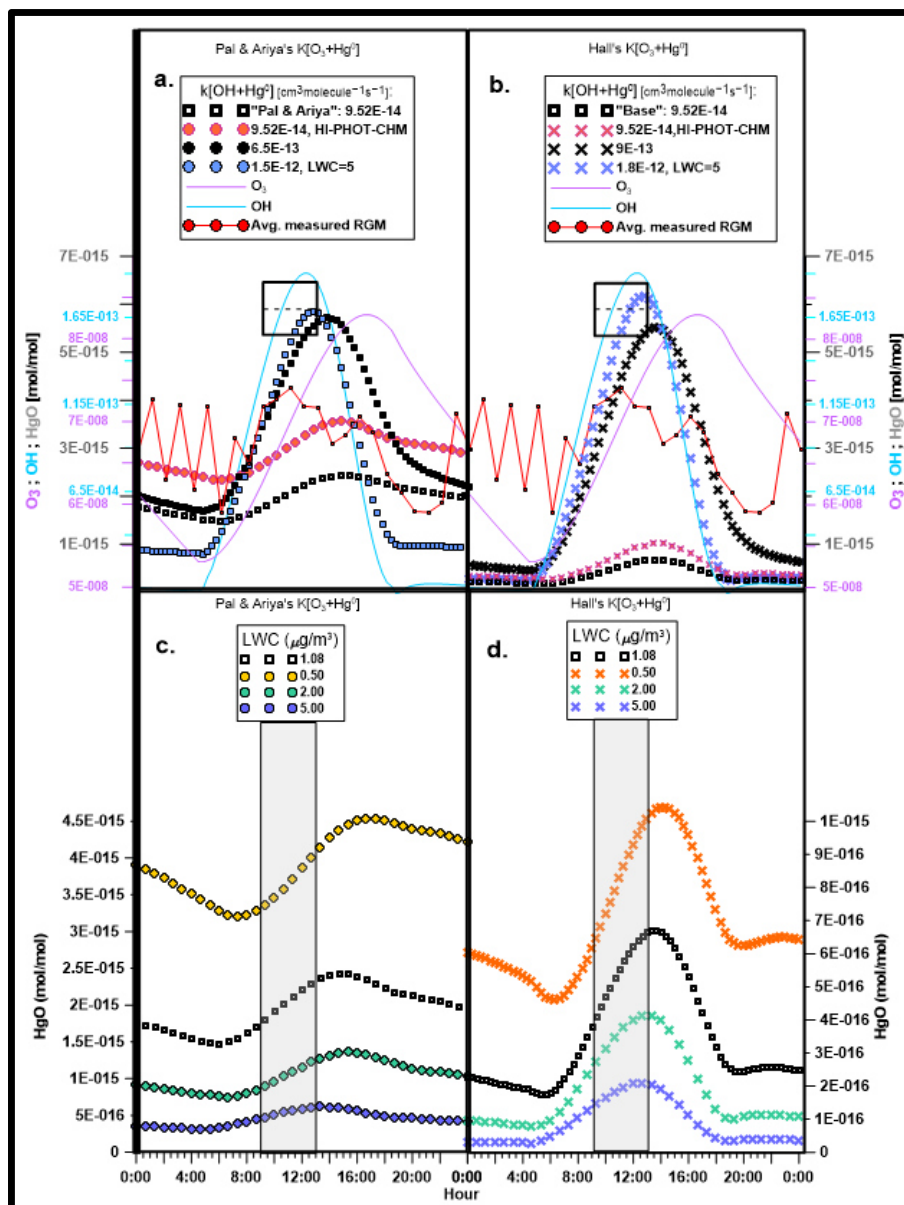
672

673

674



675



676



677 **Figure 4.** HgO concentration as a function of GEM oxidation by OH and aerosol LWC. (a) HgO
678 concentrations obtained using different $k[\text{OH}+\text{Hg}^0]$ values with Pal and Ariya's (2004b) $k[\text{O}_3+\text{Hg}^0]$, LWC =
679 $5 \mu\text{g m}^{-3}$, and $[\text{O}_3] = 120 \text{ ppb}$ (HI-PHOT-CHM), when indicated. Black squares represent PAL-ARIYA
680 scenario (see Table 1). (b) HgO concentrations obtained using different $k[\text{OH}+\text{Hg}^0]$ values with Hall's (1995)
681 $k[\text{O}_3+\text{Hg}^0]$, LWC = $5 \mu\text{g m}^{-3}$ and $[\text{O}_3] = 120 \text{ ppb}$ (HI-PHOT-CHM), when indicated. The filled boxes represent
682 the BASE scenario (see Table 1). The dashed line inside the box in the upper panels indicates the average
683 measured daytime RGM maximum and the time during which it occurred (~0900–1300 h; see Fig. 1). The
684 vertical dimension of the box in the upper panels marks the corresponding standard deviation of the mean of
685 the daytime measured RGM maximum. The lower panels present daytime HgO concentrations obtained using
686 different LWC values ($0.50\text{--}5.00 \mu\text{g m}^{-3}$) and $k[\text{O}_3+\text{Hg}^0]$ based on Pal and Ariya (2004b) (c) and on Hall
687 (1995) $k[\text{O}_3+\text{Hg}^0]$ (d). The shaded areas represent the timing of the maximal daylight RGM levels observed
688 from the average diurnal profile of RGM (~0900–1300 h; see Fig. 1).

689

690

691

692

693

694

695

696

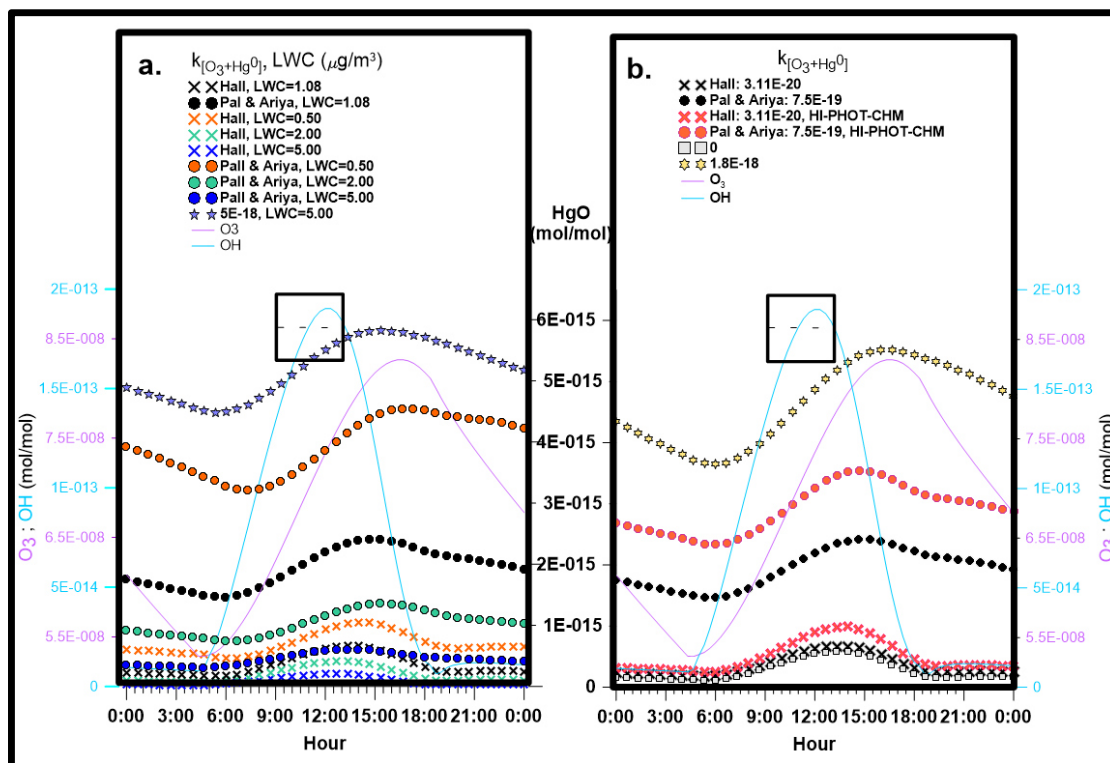
697

698



699

700



701

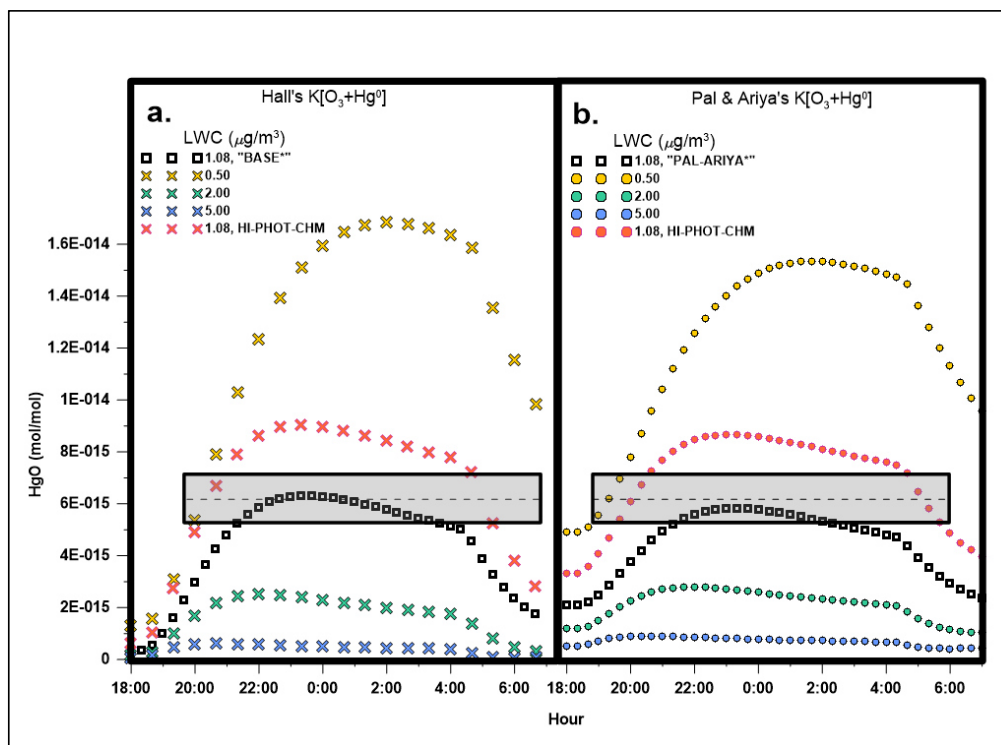
Figure 5. Dependence of HgO diurnal profile on oxidation by OH, O₃ and LWC. The figure shows the HgO concentration obtained using $k_{[OH+Hg^0]} = 9.52\text{E-}14 \text{ cm}^3 \text{ molecule}^{-1} \text{ s}^{-1}$ and different $k_{[O_3+Hg^0]}$ values and O₃ concentrations (a) and different $k_{[O_3+Hg^0]}$ values and aerosol LWCs (b). The dashed line inside the box indicates the average measured daytime RGM maximum level (5.88 ppq; see Fig. 3) and the time during which it occurred (~0900–1300 h; see Fig. 1). The vertical dimension of the box marks the corresponding standard deviation of the mean (0.53 ppq) of the measured daytime RGM maximum.

708



709

710



711

712 **Figure 6.** Simulated HgO concentration as a function of GEM oxidation rate by NO₃, O₃ concentration and
713 aerosol LWC. The width of the rectangles represents the time span of the maximal nighttime RGM (all night;
714 see Fig. 1), while the dashed line inside the rectangles denotes the average measured nighttime RGM maxima
715 (6.17 ppq) for selected nights (see text). The vertical dimension of the rectangles represents the corresponding
716 standard deviation of the mean over the measured RGM peaks (0.95 ppq). The black squares represent BASE*
717 and PAL-ARIYA* simulations, respectively (see Table 1).

718